The Astrophysical Journal, 702:L138–L142, 2009 September 10 doi:10.1088/0004-637X/702/2/L138

SOLAR MOSS PATTERNS: HEATING OF CORONAL LOOPS BY TURBULENCE AND MAGNETIC CONNECTION TO THE FOOTPOINTS

R. Kittinaradorn[1], D. Ruffolo[1,2], and W. H. Matthaeus[3]
[1] Department of Physics, Faculty of Science, Mahidol University, Bangkok 10400, Thailand; rkcosmos@gmail.com, scdjr@mahidol.ac.th
[2] ThEP Center, CHE, 328 Si Ayutthaya Road, Bangkok 10400, Thailand
[3] Bartol Research Institute and Department of Physics and Astronomy, University of Delaware, Newark, DE 19716, USA; yswhm@bartol.udel.edu
Received 2009 February 23; accepted 2009 July 31; published 2009 August 21

ABSTRACT

We address the origin of the patchy dark and bright emission structure, known as "moss," observed by TRACE extreme ultraviolet observations of the solar disk. Here we propose an explanation based on turbulent, patchy heat conduction from the corona into the transition region. Computer simulations demonstrate that magnetic turbulence in coronal loops develops a flux rope structure with current sheets near the flux rope boundaries. Localized heating due to current sheet activity such as magnetic reconnection is followed by heat conduction along turbulent magnetic field lines. The field line trajectories tend to remain near the flux rope boundaries, resulting in selective heating of the plasma in the transition region. This can explain the network of bright regions in the observed moss morphology.

Key words: Sun: corona – Sun: magnetic fields – Sun: transition region – turbulence

1. INTRODUCTION

Recent extreme ultraviolet (EUV) observations of the solar disk by TRACE have discovered "moss" emission with irregular dark and bright patches (Berger et al. 1999b). While this has been found to derive from the solar transition region at the base of hot coronal loops (Fletcher & De Pontieu 1999; Martens et al. 2000), and the emission is apparently associated with a downward heat flux from the corona (Berger et al. 1999b), the origin of the patchiness of the emission structure has not been completely clarified. One viewpoint is that the structuring of moss emission is associated with chromospheric jets observed in terms of Doppler-shifted Hα absorption. Another possibility, explored here, is that the EUV brightness is enhanced by heat transport along magnetic field lines from localized heat sources in the corona (Figure 1). Both of the leading concepts for heat production in the solar corona, i.e., dissipation of MHD waves and nanoflares, involve heating by magnetic reconnection at the boundaries of "flux ropes." We specifically examine the nature of downward heat conduction associated with heating due to turbulent MHD processes near the boundaries of coronal flux ropes. In our analysis we make use of a simple representation that captures important topological features of an evolving magnetic field in MHD in a strongly magnetized plasma with a large DC guide field. In particular, we approximate the fully three-dimensional configuration as a superposition of two-dimensional (2D) structures that are independent of distance along the mean field (the flux ropes), as well as wave-like "slab" fluctuations (here, Alfvén waves excited by solar oscillations) that propagate and vary along the mean field. It is natural to expect these fluctuations to be turbulent. Thus we propose that heating associated with current sheet activity, including reconnection, occurs along the boundary surfaces. Heat transport along these surfaces, which have a network-type topology, can explain the selective heating of plasma in the transition region and the patchy network of bright regions. We present computer simulation results to demonstrate these effects.

2. BACKGROUND

Coronal loops can be divided into two broad classes: hot coronal loops that are observed in X-rays, and cool coronal loops, observed in EUV. Broad regions of emission at the base of hot coronal loops were first noted in observations by the Normal Incidence X-ray Telescope (Peres et al. 1994). EUV observations by the TRACE satellite with improved resolution revealed that these regions have an interesting bright-dark patchy (spongy) structure, called "moss." This implies that the emission measure at the footpoints is inhomogeneous. The moss emission comes from the upper transition region, at temperatures of 0.6–1.5 MK (Fletcher & De Pontieu 1999), over a vertical thickness of 1 Mm starting from a base height of $\approx$ 1.5–2 Mm above the photosphere (Berger et al. 1999a). Moss emission is found over magnetic plages at the footpoints of coronal loops at $>$ 2 MK, and can be accounted for by conductive heat flow from the overlying loops (Fletcher & De Pontieu 1999; Martens et al. 2000; De Pontieu et al. 2003b).

In general, the locations of interior moss features are not well associated with photospheric structures. Some of the dark features, especially dark incursions from the edges, are associated with regions of Doppler-shifted-Hα jets of chromospheric material (Berger et al. 1999a; De Pontieu et al. 1999), and statistical correlations have been found spatiotemporally with chromospheric emission at the Hα line center (De Pontieu et al. 2003b), spatially with the Lyα line (Vourlidas et al. 2001), and temporally with chromospheric jets (De Pontieu et al. 2003a, 2004). While these observations, as well as simulation results (Hansteen et al. 2006; De Pontieu et al. 2007a), have been interpreted to imply that obscuration by cooler chromospheric material plays a role in determining the mottled appearance of moss, it is possible that this is not the only mechanism driving the fine structure of the moss emission. As the moss emission is believed to be due to a downward heat flux from an overlying hot coronal loop (Berger et al. 1999b), we examine selective heating of transition region material due to varying magnetic connection to strong, remote heat sources higher in the corona. One attractive feature of this view is that moss patterning is attributed to the structure of turbulence that pervades the solar atmosphere, and this turbulence can be statistically homogeneous with a large-scale magnetic field that is uniform over the "field" of moss, in agreement with the observation of Katsukawa & Tsuneta (2005) that unipolar moss regions (with boundaries defined to remove major incursions) have photospheric magnetic field strengths

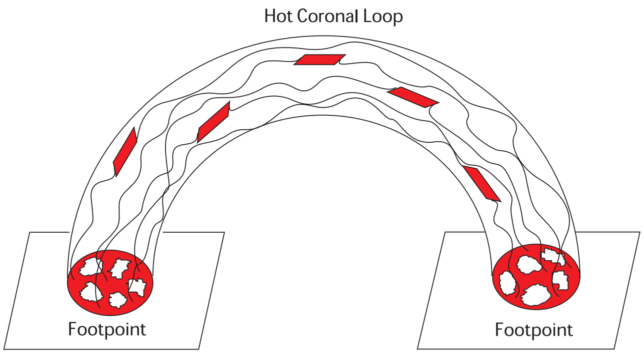

Figure 1. Illustration of reconnection structures that are expected to occur in turbulence within a coronal loop. In this model, heating occurs at these planar structures. The heat transport is predominantly along magnetic field lines, which map onto network-like patterns at the footpoints to produce bright "moss" features in the transition region.

and orientations that are quite uniform across both dark and bright regions.

Our work is motivated in part by an analogous and widely accepted explanation of "dropouts" of solar energetic particles from impulsive solar flares, in which patchy structures with a presence or absence of particles in interplanetary space are attributed to magnetic connection with the localized flare source (Mazur et al. 2000; Giacalone et al. 2000) or more specifically to temporary trapping of field lines due to the turbulence topology (Ruffolo et al. 2003; Zimbardo et al. 2004) and suppressed diffusive escape from trapping (Chuychai et al. 2005, 2007; Tooprakai et al. 2007). Images of moss indeed appear visually similar to simulated distributions of impulsive flare particles in interplanetary space.

To pursue this idea, we trace the magnetic field lines from reconnection regions that appear in turbulence (assumed to be in the corona) to the footpoints (assumed to be the transition region) to show that the bright-dark structure can be explained by nonuniformity of field line transport in magnetic turbulence.

3. MODEL AND PROCEDURE

Magnetic turbulence. In a low beta plasma threaded by a strong mean magnetic field we expect a high degree of anisotropy, and to leading order we expect the dominant low frequency nonlinear behavior to involve fluctuations that vary much more rapidly across the mean magnetic field than along it. In terms of a wave vector description, we expect the cascade associated with the turbulence to mainly excite small-scale structures with large wave vectors $k_\perp$ perpendicular to the mean field. A smaller amount of energy may be found in parallel wave vectors $k_\parallel$. A simple way of describing such turbulent fluctuations to a first approximation is as a 2D spectrum of fluctuations, with nonzero $k_\perp$ but $k_\parallel = 0$, to which we may add an ingredient of parallel propagating fluctuations, having $k_\perp = 0$ and nonzero $k_\parallel$. This kind of two-component model, though highly oversimplified, captures in a descriptive way the essential features of anisotropy, while maintaining a fully three-dimensional magnetic field. It has been very useful, for example, in the theory of interplanetary pitch angle scattering of energetic charged particles (Bieber et al. 1994; Shalchi et al. 2008). The 2D component usually accounts for most of the energy, and is very similar to the Reduced MHD model (Strauss 1976; Montgomery 1982; Zank & Matthaeus 1991) which has frequently been used as a simple representation of coronal loop and flux tube dynamics (Einaudi et al. 1996; Hendrix & Van Hoven 1996; Dmitruk & Gomez 1997).

In the present model we begin with a magnetic field obtained from a 2D spectral method simulation. We adopt a Cartesian geometry, as the small-scale, patchy pattern of magnetic connection to heating regions is unlikely to be significantly deformed by the loop curvature. We first generate a potential function $a(x,y)$ from its power spectrum,

$$A(k_\perp) \propto \frac{1}{\left(1 + k_\perp^2 \lambda_\perp^2\right)^{7/3}}, \tag{1}$$

with random phases (see Figure 2(a)). This leads to an omnidirectional magnetic power spectrum with a Kolmogorov power law in the inertial range and a $k_\perp^3$-dependence in the energy-containing range as required for homogeneity (Ruffolo et al. 2004; Matthaeus et al. 2007). We can then define the 2D magnetic field by $\mathbf{b}^{2D}(x, y) = \nabla \times [a(x, y)\hat{\mathbf{z}}]$, where $\hat{\mathbf{z}}$ is the direction of the uniform DC guide magnetic field. Note that $\mathbf{b}^{2D} \perp \nabla a(x, y)$, so the 2D field follows contours of constant a. Adding the DC guide field, the combined magnetic field twists along flux surfaces defined by the contours of constant a. In the simulations, the magnetic field is determined in wave vector space, and after a 2D fast Fourier transform (FFT) we arrive at the real space representation, with 1024 points in each direction (x and y), corresponding to a width of 40 Mm. Then a 2D pseudospectral incompressible MHD code is employed to advance the magnetic configuration in time. The simulation has 1024^2 spatial resolution and a magnetic Reynolds number of 640 at the largest scales.

For the 2D magnetic field, Figure 2 illustrates contours of the magnetic potential function, i.e., cross-sections of flux surfaces, for (a) the initial conditions, which have random phases and a specified spectrum, and (b) after 2D MHD evolution for approximately one nonlinear time, when coherent current structures have formed and nonlinear relaxation processes have commenced. Whereas the initial conditions have irregular contours of varying separation, after the 2D MHD evolution the contours are for the most part evenly spaced, indicating that the magnetic field magnitude (and magnetic pressure) is more uniform, except at the "topological defects," i.e., current structures, highlighted in white and blue in Figure 2(b). The evolution between $t = 0$ and $t \sim 1$ (approximately one eddy turnover time at the energy containing scale) as seen in Figure 2 is similar to the scenario described by Matthaeus & Montgomery (1980). 2D MHD exhibits a dual cascade of magnetic excitation to larger scales (lower wavenumbers) and current density to smaller-scale, coherent structures (at higher wavenumbers) that would not be obtained with a random phase model as used for the initial conditions for this run.

We complete the model magnetic field by adding fluctuations with parallel wave vectors ($\mathbf{k} \parallel \hat{\mathbf{z}}$, i.e., "slab" turbulence") that represent standing waves and counter-propagating Alfvén waves (Aschwanden 2004; Tomczyk et al. 2007; De Pontieu et al. 2007b). Such waves would typically be driven by photospheric oscillations, which have a peak power corresponding to the 5-minute period of p-mode oscillations. However, that period corresponds to a wavelength longer than a typical loop, with slow motions of the entire coronal loop that do not significantly distort the relative, small-scale pattern of magnetic connectivity. The slab fluctuations with wavelengths of a fraction of the loop length are driven by high-frequency oscillations, where the power spectrum has a power-law dependence on frequency and wavenumber (Libbrecht 1988). Therefore, we introduce the

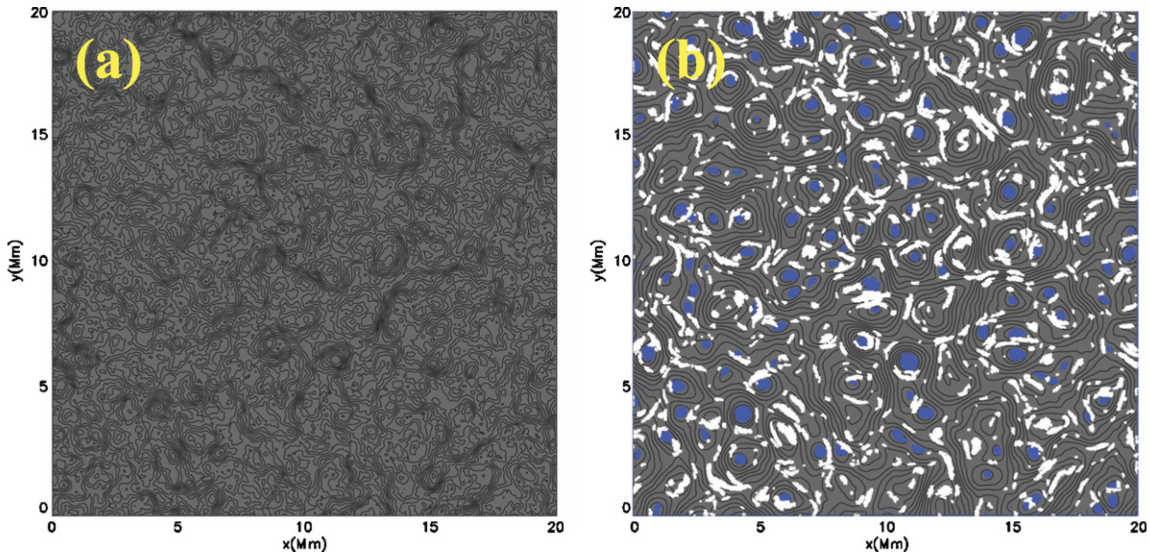

Figure 2. Contours of equal magnetic potential (flux surfaces) for 2D turbulence models: (a) a realization with random phases of Fourier components, and (b) that realization after evolution through a 2D MHD code over an eddy turnover time at the outer scale. These coordinates (x, y) correspond to a 2D cross-section through the coronal flux rope. In this model, heating occurs at current sheets attributed to reconnection (white), corresponding to planes in three dimensions (Figure 1). Note also the current cores (blue) near O-points, particularly in smaller topological islands.

slab component using a discrete, turbulent power-law spectrum ($P \propto k^{-5/3}$), normalized so that the energy in the slab component is 20% of the total 2D+slab magnetic fluctuation energy. This fraction is motivated by the slab fraction observed in interplanetary magnetic fluctuations (Bieber et al. 1994, 1996). The ratio of fluctuation and mean field amplitudes is $b/B_0 = 0.5$. Again an FFT is used to obtain the real-space magnetic field. The transform in z used $2^{22} = 4.2 \times 10^6$ points, corresponding to a length of 400 Mm; in practice, field lines are traced for only a small fraction of that length in order to avoid periodicity effects. In our simulations, the slab component represents a small fraction of the total fluctuation energy, and plays only a minor role in defining the patterns of magnetic connection to heat sources. However, it does render the full fluctuation field three-dimensional, so that magnetic field lines can cross the flux surfaces defined by constant $a(x, y)$ (Chuychai et al. 2007), and no coordinate is ignorable. Therefore, including the slab component increases the realism of the magnetic field model by eliminating anomalies such as spurious conserved quantities that arise in fields of reduced dimensionality (e.g., Jokipii et al. 1993).

Coronal heating, wave heating, and current sheets. In a low beta anisotropic plasma, the coherent current structures that form due to a turbulent cascade can be classified into two types of structures (Matthaeus & Lamkin 1986; Greco et al. 2009), namely current cores and current sheets. The former are the currents required by Faraday's law to support a simple flux tube with a single signed helicity. In terms of the topology of the 2D turbulence, the current cores are close to O-points. It turns out that MHD turbulence leads to the formation of many such tubes and at every stage of evolution they relax locally while interacting with one another at their boundaries (Servidio et al. 2008). The current sheets are found at the boundaries between flux tubes where regions of locally relaxing plasma encounter one another. The current sheets are candidates for magnetic reconnection and heating, both of which may be related to plasma kinetic and wave processes including anomalous resistivity. The tendency to form the current sheets is, however, firmly rooted in MHD.

After our 2D MHD simulation, we trace magnetic field lines from initial locations within high-current regions, which include both the current sheets, which are likely sites of plasma heating, and current cores. In our model of the coronal loop, the field lines are heated by ohmic dissipation, and a disproportionate fraction of this heating occurs at current sheets including those undergoing reconnection. Therefore identification of high-current-density regions is crucial to our model. In a more realistic kinetic plasma model, it is likely that the high-current regions would again be sites of enhanced heating, but possibly by different processes that are operative in a low-collisionality plasma. In our simulations, we calculated the current density at each grid point and decided on a threshold. For any grid point that has a high current density, i.e., above the threshold, one initial location for field line tracing is assigned to a random location within the cell surrounding the grid point. With this method, we trace 28,797 field lines from the high-current regions in a 20×20 Mm^2 area (Figure 3(a)).

In our example MHD simulation the current sheets are readily identified visually; see the white regions in Figures 2(b) and 3(a). These thin structures are planes in three dimensions (see Figure 1). Heating at current sheets in 2D magnetic turbulence is conceptually similar to models invoking nanoflares between colliding flux ropes (Parker 1988). Thus in MHD turbulence, the competing ideas of coronal heating due to flux rope reconnection and wave dissipation converge toward a single composite picture. The current cores in Figures 2(b) and 3(a) are colored blue. Their intensity and gradients are much more gentle than those of current sheets. At high magnetic Reynolds number we do not expect significant heating in the cores, nor should they be sites of strong anomalous resistivity in a picture augmented by kinetic plasma processes.

Computation of Magnetic Field Line Trajectories. Finally, to model heat transport due to electron flow along magnetic field lines, we trace individual magnetic field lines from the selected set of initial locations to higher z, i.e., down the coronal loop for a variable distance toward the footpoint, by solving the coupled differential equations for field line trajectories using a fourth-order Runge–Kutta method with adaptive time stepping (Press

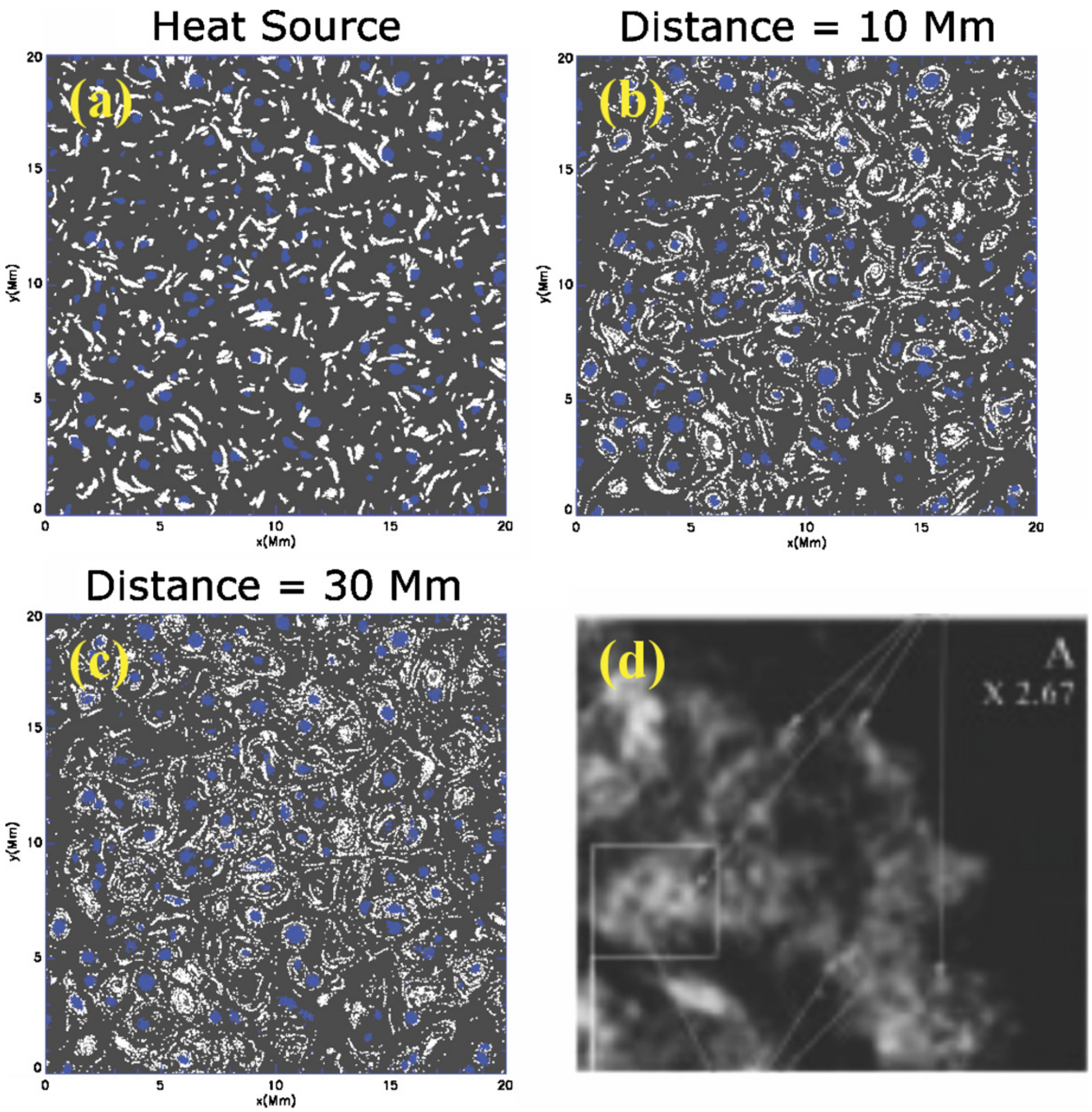

Figure 3. (a) Random initial locations of nearly 30,000 field lines within regions of high current, in current sheets (white) or current cores (blue). The same field lines traced through the magnetic turbulence over a distance of (b) 10 Mm or (c) 30 Mm. (d) Observed moss features, from Figure 1 of Berger et al. (1999a).

et al. 1992). The equations are

$$\frac{dx}{dz} = \frac{b_x(x, y, z)}{B_0}, \quad \frac{dy}{dz} = \frac{b_y(x, y, z)}{B_0}. \tag{2}$$

Note that **b** is determined by interpolation from neighboring grid points (linear interpolation for the slab component and bilinear interpolation for the 2D component). The field lines are then traced to various distances z. More realistically, each field line should be thought of as representative of a thin flux bundle.

4. RESULTS

Figure 3 shows results of a field line tracing numerical experiment, compared with observations. Figure 3(a) shows the selected initial locations of magnetic field lines (current cores in blue and current sheets in white), i.e., their locations at the heat source. The distributions of the current cores and current sheets are highly structured from the outset. As we trace the magnetic field lines downward, they spread to form a broader distribution, but mostly remain on the same flux surfaces. In particular, the field lines from current sheets, where heating is expected to occur, remain near the edges of flux ropes. The distribution evolves quite rapidly, and after the relatively short distance z of 10 Mm, the distribution of heated field lines (white regions in Figure 3(b)) already has a mottled appearance.

At $z = 30$ Mm, the distribution of heated field lines takes on more of a network topology (with dark cores) that is qualitatively similar to moss (Figure 3(c)). For a visual comparison, Figure 3(d) shows an image of moss observations to the same scale.[4] For greater distances z (up to 200 Mm), the distribution does not change significantly. Thus we interpret that $z = 30$ Mm is the approximate minimum height from which coronal heating can lead to moss patterns with a network topology. This may constrain the ability of our model to explain network-type moss in certain cases; for particularly short loops we would expect coherent patches associated with the initial pattern of heating. This

[4] With kind permission from Springer Science+Business Media: from Figure 1 of Berger et al. (1999a).

distance scale may also have implications regarding locations of reconnection heating in coronal loops.

The distance over which a network topology develops has been examined by computer simulations for $\lambda_\perp = 1.5$, 0.5, and 0.25 Mm, and for $b/B_0 = 0.5$ and 0.05. That distance appears to vary inversely with b/B_0, i.e., the evolution requires a longer distance for weaker turbulence. Surprisingly, this distance seems to be insensitive to $\lambda_\perp$ over the range examined (varying by a factor of 6).

The best match with observations is obtained for $\lambda_\perp = 0.5$ Mm, the case shown in Figure 3. Other than that, the simulation is not "tuned" to model a specific observational data set. It is not surprising that the bright patches in actual solar moss are "fuzzy" or "blurred" with respect to this basic simulation model, for various reasons: (1) We trace a finite number of discrete field lines, whereas the actual mapping of the current sheets down to the footpoint according to magnetic connection would be a highly branched but continuous region (Similon & Sudan 1989). (2) The bright patches should receive contributions from a magnetic connection mapping over a range of z values as opposed to the single value displayed here. (3) In addition to heat transport by electron flow along the field lines, there is some transport of electrons across field lines (Galloway et al. 2006). (4) The observed moss features are not resolved by TRACE observations.

5. CONCLUSIONS

In conclusion, the patchy distribution of moss emission in the solar transition region can be explained in terms of heat sources at strong MHD current sheets in the overlying coronal loops, followed by heat transport along turbulent magnetic field lines. According to numerical simulations, in comparison with observations, the magnetic turbulence in the coronal loop should have a scale length of ~ 0.5 Mm perpendicular to the mean DC guide field. After evolution through a 2D MHD simulation, current sheets naturally form near the edges of flux surfaces of the 2D field component. The locus of magnetic field lines connected to the heat source spreads around the flux surfaces, giving rise to a network of heated regions that resembles moss emission patterns, particularly after a distance of ~ 30 Mm. As it has already been proposed that moss emission is associated with a downward heat flux from overlying hot coronal loops (Berger et al. 1999b), here we point out that the likely distribution of heat sources and heat transport along turbulent magnetic field lines can naturally explain the patchy morphology of the moss.

This work was supported by the Junior Science Talent Project (JSTP) of the National Science and Technology Development Agency (NSTDA) of Thailand, the Sritrang Thong Project of the Faculty of Science at Mahidol University, the Thailand Research Fund, NASA Grant NNG05GG83G, the NASA Heliophysics Theory program, NASA NNX08AI47G, and the SHINE program, NSF ATM0752135.

REFERENCES

Aschwanden, M. J. 2004, Physics of the Solar Corona (Chichester: Springer-Praxis)
Berger, T. E., De Pontieu, B., Fletcher, L., Schrijver, C. J., Tarbell, T. D., & Title, A. M. 1999a, Sol. Phys., 190, 409
Berger, T. E., De Pontieu, B., Schrijver, C. J., Tarbell, T. D., & Title, A. M. 1999b, ApJ, 519, L97
Bieber, J. W., Matthaeus, W. H., Smith, C. W., Wanner, W., Kallenrode, M.-B., & Wibberenz, G. 1994, ApJ, 420, 294
Bieber, J. W., Wanner, W., & Matthaeus, W. H. 1996, J. Geophys. Res., 101, 2511
Chuychai, P., Ruffolo, D., Matthaeus, W. H., & Meechai, J. 2007, ApJ, 659, 1761
Chuychai, P., Ruffolo, D., Matthaeus, W. H., & Rowlands, G. 2005, ApJ, 633, L49
De Pontieu, B., Berger, T. E., Schrijver, C. J., & Title, A. M. 1999, Sol. Phys., 190, 419
De Pontieu, B., Erdélyi, R., & de Wijn, A. G. 2003a, ApJ, 595, L63
De Pontieu, B., Erdélyi, R., & James, S. P. 2004, Nature, 430, 536
De Pontieu, B., Hansteen, V. H., Rouppe van der Voort, L., van Noort, M., & Carlsson, M. 2007a, ApJ, 655, 624
De Pontieu, B., Tartell, T., & Erdélyi, R. 2003b, ApJ, 590, 502
De Pontieu, B., et al. 2007b, Science, 318, 1574
Dmitruk, P., & Gomez, D. 1997, ApJ, 484, L83
Einaudi, G., Velli, M., Politano, H., & Pouquet, A. 1996, ApJ, 457, L113
Fletcher, L., & De Pontieu, B. 1999, ApJ, 520, L135
Galloway, R. K., Helander, P., & MacKinnon, A. L. 2006, ApJ, 646, 615
Giacalone, J., Jokipii, J. R., & Mazur, J. E. 2000, ApJ, 532, L75
Greco, A., Matthaeus, W. H., Servidio, S., Chuychai, P., & Dmitruk, P. 2009, ApJ, 691, L111
Hansteen, V. H., De Pontieu, B., Rouppe van der Voort, L., van Noort, M., & Carlsson, M. 2006, ApJ, 647, L73
Hendrix, D. L., & Van Hoven, G. 1996, ApJ, 467, 887
Jokipii, J. R., Kota, J., & Giacalone, J. 1993, Geophys. Res. Lett., 20, 1759
Katsukawa, Y., & Tsuneta, S. 2005, ApJ, 621, 498
Libbrecht, K. G. 1988, ApJ, 334, 510
Martens, P. C. H., Kankelborg, C. C., & Berger, T. E. 2000, ApJ, 537, 471
Matthaeus, W. H., Bieber, J. W., Ruffolo, D., Chuychai, P., & Minnie, J. 2007, ApJ, 667, 956
Matthaeus, W. M., & Lamkin, S. L. 1986, Phys. Fluids, 29, 2513
Matthaeus, W. H., & Montgomery, D. C. 1980, Ann. N. Y. Acad. Sci., 357, 203
Mazur, J. E., Mason, G. M., Dwyer, J. R., Giacalone, J., Jokipii, J. R., & Stone, E. C. 2000, ApJ, 532, L79
Montgomery, D. 1982, Physica Scripta, T2, 83
Parker, E. N. 1988, ApJ, 330, 474
Peres, G., Reale, F., & Golub, L. 1994, ApJ, 422, 412
Press, W. H., Teukolsky, S. A., Vetterling, W. T., & Flannery, B. P. 1992, Numerical Recipes in FORTRAN: The Art of Scientific Computing (Cambridge: Cambridge Univ. Press)
Ruffolo, D., Matthaeus, W. H., & Chuychai, P. 2003, ApJ, 597, L169
Ruffolo, D., Matthaeus, W. H., & Chuychai, P. 2004, ApJ, 614, 420
Servidio, S., Matthaeus, W. H., & Dmitruk, P. 2008, Phys. Rev. Lett., 100, 095005
Shalchi, A., Bieber, J. W., & Matthaeus, W. H. 2008, A&A, 483, 371
Similon, P. L., & Sudan, R. N. 1989, ApJ, 336, 442
Strauss, H. 1976, Phys. Fluids, 19, 134
Tomczyk, S., McIntosh, S. W., Keil, S. L., Judge, P. G., Schad, T., Seeley, D. H., & Edmondson, J. 2007, Science, 317, 1192
Tooprakai, P., Chuychai, P., Minnie, J., Ruffolo, D., Bieber, J. W., & Matthaeus, W. H. 2007, Geophys. Res. Lett., 34, L17105
Vourlidas, A., Klimchuk, J. A., Korendyke, C. M., Tarbell, T. D., & Handy, B. N. 2001, ApJ, 563, 374
Zank, G. P., & Matthaeus, W. H. 1991, Phys. Fluids, 3, 69
Zimbardo, G., Pommois, P., & Veltri, P. 2004, J. Geophys. Res., 109, A02113